# Applying Numerical Methods to Fluid Structure Interactions in Biological Systems

Courtney Chancellor
Department of Mathematics
Southern Methodist University

**Project Mentors**
Dr. Padmanabhan Seshayier
Dr. Daniel Anderson

## Abstract

This undergraduate research presents mathematical and numerical modeling of intracranial saccular aneurysms. The blood pressure acting on the arterial wall is modeled using a Fourier Series, the arterial wall by a spring mass system, and the cerebral spinal fluid by a simplified Navier Stokes equation. The resulting partial differential equation for this fluid structure interaction is solved numerically using the implicit finite difference method. Computational studies are also presented, observing the influence of various parameters on the overall behavior of the system.

This final report is submitted in partial fulfillment of the
National Science Foundation REU and Department of Defense ASSURE Program
George Mason University
June 1, 2009 - July 31, 2009

# 1 Introduction

The health industry has in recent years become one of the fastest growing and most stable in America, fueled by an aging population and swell of scientific development. Some of the greatest pressures are those for the advancement of faster, more accurate diagnosis, the reduction of invasive procedures, and cost-effective treatment plans. Meeting these goals requires a multidisciplinary approach, combining the expertise of science, mathematics, and the humanities. The focus of this paper will be the modeling of fluid structure interactions, specifically those of intracranial saccular aneurysms. A focal dilatation of an arterial wall, aneurysms are surprisingly common with an estimated two to five percent of Americans harboring intracranial, or cerebral, aneurysms. Bulging from the arterial wall, aneurysms may interrupt blood flow, put pressure on nerve or brain tissue, or rupture, causing hemorrhage.

Within the study of aneurysms, there are three general topics one can address: pathogenesis, enlargement, and rupture. Pathogenesis concerns itself mainly with the cause of aneurysm development. Little is known as to what causes these weaknesses in the vessel wall, however, research has linked their development to genetic predispositions, cardiovascular trauma, and medical conditions as common as high blood pressure and atherosclerosis. Subjected to the force of the blood pressure, an aneurysm tends to enlarge over time. However, this enlargement varies with age, gender, blood chemistry and can be unpredictable in its rate of growth. Perhaps the most crucial research to the immediate improvement in aneurysm treatment is that pertaining to rupture. Unruptured, even the largest of aneurysms can be benign. Upon rupture, however, forty percent of patients will die within the first twenty four hours and twenty five percent within the subsequent six months [1,5]. Of the surviving patients, many will experience extensive neural damage. The only treatments currently available for intracranial saccular aneurysms tend to be either highly invasive or must be repeated every few years. While the vast majority

of aneurysms will never rupture, the combined risk of surgery and the fatal consequences of rupture leave many health care providers uncertain as to what may be the best care they can give their patients.

One possible reason for the enlargement and eventual rupture of an intracranial aneurysm is that the dynamic behavior of the arterial wall is unstable in response to the pulsatile blood flow and surrounding cerebral spinal fluid. The construction of a mathematical model and the derivation of an exact solution exists in previous research[7], but a numerical solution to the problem has not been investigated. In this paper, numerical methods in the form of implicit finite differences have been applied to the problem, allowing for the future modification of its individual components. Ultimately, we attempt to contribute to a mathematical model which would assist physicians in the care and choice of treatment in aneurysm patients.

## 2 Background and Research Methods

The studied model contains three components of intracranial saccular aneurysms: the blood pressure acting on the inner arterial wall, the structure of the arterial wall itself, and the surrounding cerebral spinal fluid (CSF). To begin, we consider the simplest case of a perfectly spherical aneurysm. Due to radial symmetry [6], the model is immediately brought from three dimensions to one, as determining the motion of the wall in one direction will determine its behavior in all directions. We can visualize this as a line running from inside the aneurysm, through the arterial wall and into the CSF, with the point $x = 0$ set where the outer arterial wall and CSF meet. $x > 0$ will be considered to be moving away from the wall and into the CSF and $x < 0$ moving through the wall and into the bloodstream.

While there are many ways to represent each of the three components in this model, we chose the following to mimic preexisting research for which an exact solution has been

determined.

## 2.1 Model of the blood pressure

Blood pressure, being pulsatile, will be modeled by the Fourier series[2,3].

$$P_{\text{blood}} = P_m + \sum_{n=1}^{N} (A_n \cos(n\omega t) + B_n \sin(n\omega t)) \tag{1}$$

where $P_m$ is the mean blood pressure, $A_n$ and $B_n$ are the Fourier coefficients for N harmonics, and $\omega$ is the fundamental circular frequency.

## 2.2 Model of the arterial wall

The arterial wall will be modeled using the familiar spring and mass system as illustrated in Figure 1. This will mimic the elasticity of the arterial wall and the coupled motion of its inner and outer components while maintaining simplicity. $k$ is defined as the spring constant and $m$ as the mass. Ultimately, it is the motion of the outer wall and its interaction with the CSF with which we will be most concerned.

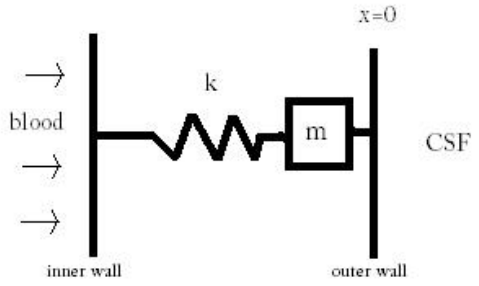


Figure 1: Diagram of Spring Mass System

## 2.3 Model of cerebral spinal fluid

The cerebral spinal fluid will be represented by the following equation:

$$\rho v_t + \rho v v_x + P_x - \mu v_{xx} = F \tag{2}$$

This, the one dimensional Navier -Stokes equation, is a standard in modeling fluid interactions and has been extensively studied by mathematicians. Here, $\rho$ is the fluid density, $v(x,t)$ is the velocity of the fluid, $P(x,t)$ is the pressure of the fluid, $\mu$ is the viscosity and $F$ is the body force on the fluid. To incorporate the CSF's interaction with the arterial wall, a new variable, $u(x,t)$, representing the displacement of the cerebral spinal fluid is introduced. This variable can be related to the fluid velocity term, $v(x,t)$ by the following:

$$u = \int v dt \tag{3}$$

To make further simplifications to this model we assume that the CSF is inviscid, or an ideal fluid ($\mu = 0$). That is, that the fluid has no internal resistance to flow. We will also assume that the nonlinear effects are negligible, dropping the $\rho v v_x$ term. Two unknowns remain: pressure ($P$) and displacement ($u$). By taking the CSF to be slightly compressible, we obtain the relationship

$$P = -\rho c^2 u_x \tag{4}$$

Applying the aforementioned assumptions to the Navier-Stokes equation simplifies it to the wave equation.

$$u_{tt} = c^2 u_{xx} \tag{5}$$

For initial conditions, we assume the system starts at rest with no initial velocity,

$$u(x,0) = u_t(x,0) = 0 \tag{6}$$

To solve the coupled partial differential equation we will need two boundary conditions. At $x = 0$, the edge of the outer arterial wall, we will utilize a force balance equation which takes into account the force of the blood pressure and its effects on the spring mass system describing the arterial wall.

$$mu_{tt}(0,t) = aP_{\text{blood}} - ku(0,t) + \rho c^2 a u_x(0,t) \tag{7}$$

For the second boundary condition, we will fabricate a point $x = L$, some long distance away from the outer wall at which the waves created by the motion of the artery die down. We have chosen to use the plane wave approximation given by

$$u_t(L,t) = -cu_x(L,t) \tag{8}$$

## 2.4 The PDE

The mathematical models previously defined can be summarized as the following coupled fluid-structure interaction problem and PDE:

$$u_{tt} = c^2 u_{xx} \tag{9}$$

$$u(x,0) = 0 \qquad u_t(x,0) = 0 \tag{10}$$

$$mu_{tt}(0,t) = aP_{\text{blood}} - ku(0,t) + \rho c^2 a u_x(0,t) \tag{11}$$

$$u_t(L,t) = -cu_x(L,t) \tag{12}$$

## 2.5 Solving using implicit finite differences

We have chosen to use finite differences to solve the above PDE. When the system is discritized explicitly, using finite differences, we see

$$\left(\frac{u_i^{n+1} - 2u_i^n + u_i^{n-1}}{\delta t^2}\right) = c^2 \left(\frac{u_{i+1}^n - 2u_i^n + u_{i-1}^n}{\delta x^2}\right) \tag{13}$$

Moving all n+1 terms to the left hand side,

$$2(1-r)u_i^n + r(u_{i+1}^n + u_{i-1}^n) - u_i^{n-1} = u_i^{n+1} \tag{14}$$

where r=$\left(\frac{c^2\delta t^2}{\delta x^2}\right)$, $\delta t$ is the step size in time and $\delta x$ is the step size in space. Certain values of r will cause this matrix to become either nilpotent or contain a complete set of negative eigenvalues, leading to stability problems during vector multiplication. Thus restrictions must be placed on the time step. As we will see, implicit discritization eliminates this issue. Implicit methods, however, correspond to the form $Au^{n+1} = b$ which requires an eventual linear system solve at each time step (e.g. a blackslash command in Matlab). This uses significantly more processing power and time than explicit methods, especially for significantly small $\delta t$ and $\delta x$.

To solve this PDE, we chose to use finite differences, discritizing implicitly as outlined by

$$\left(\frac{u_i^{n+1} - 2u_i^n + u_i^{n-1}}{\delta t^2}\right) = c^2\left(\frac{u_{i+1}^{n+1} - 2u_i^{n+1} + u_{i-1}^{n+1}}{\delta x^2}\right) \tag{15}$$

where i=0,1,2...M denotes space and n=01,2,...finaltime denotes time on a grid such that $u_i^n = u(x_i, t_n)$ Note that the $u_{xx}$ term is discritized at the n+1 time level, which gives our implicit formulation.

To simplify, we move all future time step terms, or n+1 terms, to the left hand side:

$$(1+2r)u_i^{n+1} - r(u_{i+1}^{n+1} + u_{i-1}^{n+1}) = 2u_i^n - u_i^{n-1} \tag{16}$$

with $r = \frac{c^2\delta t^2}{\delta x^2}$. Here we note that the far left and right steps in space, i=0 and i=M, will be controlled by the left and right boundary conditions.

At x=0 (i=0) for all time steps we take the right boundary condition (11) and discritize, using a backward difference method which is derived from a Taylor expansion [4]for the $u_x$ term and center differences for second derivatives in time and space

$$
\begin{aligned}
mu_{tt}(0,t) = \quad & aP_{\text{blood}} && -ku(0,t) + \rho c^2 a u_x(0,t) \\
m\left(\frac{u_i^{n+1} - 2u_i^n + u_i^{n-1}}{\delta t^2}\right) \quad & = && \rho c^2 a\left(\frac{-3u_i^{n+1} + 4u_{i+1}^{n+1} - u_{i+2}^{n+1}}{2\delta x^2}\right) - ku_i^{n+1} + F(t) \\
\left(\frac{m}{\delta t^2} + \frac{3\rho c^2 a}{2\delta x} + s\right) u_0^{n+1} + \left(\frac{-2\rho c^2 a}{\delta x}\right) u_1^{n+1} \quad & + && \left(\frac{\rho c^2 a}{2\delta x}\right) u_2^{n+1} = \frac{2m}{\delta t^2} u_0^n - \frac{m}{\delta t^2} u_0^{n-1} + F(t)
\end{aligned}
$$

At x=L (i=M) for all time steps, we similarly take the left boundary condition (12) and discritize

$$
\begin{aligned}
u_t(L,t) \quad & = && -cu_x(L,t) \\
\frac{u_i^{n+1} - u_i^{n-1}}{2\delta t} \quad & = && -c\left(\frac{3u_i^{n+1} - 4u_{i-1}^{n+1} + u_{i-2}^{n+1}}{2\delta x}\right) \\
\left(\frac{1}{2\delta t} + \frac{3c}{2\delta x}\right) u_M^{n+1} - \quad & \left(\tfrac{2c}{\delta x}\right) u_{M-1}^{n+1} && + \left(\frac{c}{2\delta x}\right) u_{M-2}^{n+1} = \frac{1}{2\delta t} u_M^{n-1}
\end{aligned}
$$

To solve for interior points, we iterate the implicit discritization of the wave equation from i=1 to M-1. From this, a distinct pattern emerges which can be translated into a linear system of equations and can be solved using matrix functions. Iterating i, we produce

$$
\begin{aligned}
i = 1 \qquad & (1+2r)u_1^{n+1} - r(u_2^{n+1} + u_0^{n+1}) = 2u_1^n - u_1^{n-1} \\
i = 2 \qquad & (1+2r)u_2^{n+1} - r(u_3^{n+1} + u_1^{n+1}) = 2u_2^n - u_2^{n-1} \\
i = 3 \qquad & (1+2r)u_3^{n+1} - r(u_4^{n+1} + u_2^{n+1}) = 2u_3^n - u_2^{n-1} \\
\ldots\ldots & \\
i = M-2 \qquad & (1+2r)u_{M-2}^{n+1} - r(u_{M-1}^{n+1} + u_{M-3}^{n+1}) = 2u_{M-2} - u_{M-2}^{n-1} \\
i = M-1 \qquad & (1+2r)u_{M-1}^{n+1} - r(u_M^{n+1} + u_{M-2}^{n+1}) = 2u_{M-1}^n - u_{M-1}^{n-1}
\end{aligned}
$$

Here we notice that for n=0, terms such as $u_i^{n-1}$ arise, which as of yet have no real value

nor physical significance. To solve these equations we make an assumption that the initial velocity of the fluid is 0. This makes physical sense in the context of our initial conditions of having the entire system at rest. Thus,

$$\begin{aligned} u_t(x,0) &= 0 \\ \frac{u_i^1 - u_i^{-1}}{2\delta t} &= 0 \\ u_i^1 &= u_i^{-1} \end{aligned}$$

Applying both this equation and $u_i^0 = 0$ (derived from the initial condition), we are able to construct the following linear system of equations for n=0 which solve for the first time step.

$$\begin{aligned}
i = 0 \qquad & \left(\frac{2m}{\delta t^2} + \frac{3\rho c^2 a}{2\delta x} + k\right) u_0^1 + \left(\frac{-2\rho c^2 a}{\delta x}\right) u_1^1 + \left(\frac{\rho c^2 a}{2\delta x}\right) u_2^1 = F(t) \\
i = 1 \qquad & (2+2r)u_1^1 - r(u_2^1 + u_0^1) = 0 \\
i = 2 \qquad & (2+2r)u_2^1 - r(u_3^1 + u_1^1) = 0 \\
i = 3 \qquad & (2+2r)u_3^1 - r(u_4^1 + u_2^1) = 0 \\
.... \qquad & \\
i = m-2 \qquad & (2+2r)u_{m-2}^1 - r(u_{m-1}^1 + u_{m-3}^1) = 0 \\
i = m-1 \qquad & (2+2r)u_{m-1}^1 - r(u_m^1 + u_{m-2}^1) = 0 \\
i = m \qquad & \left(\frac{3c}{2\delta x}\right) u_m^1 - \frac{2c}{\delta x} u_{m-1}^1 + \frac{c}{2\delta x} u_{m-2}^1 = 0
\end{aligned}$$

This can be transformed to the corresponding sparse matrix system

$$\begin{bmatrix} A_0 & B & C & & & \\ 2+2r & -r & & & & \\ -r & 2+2r & -r & & & \\ & \ddots & \ddots & \ddots & & \\ & & -r & 2+2r & -r & \\ & & D & E & F_0 & \end{bmatrix} \vec{u_i^1} = \begin{bmatrix} F(t) \\ 0 \\ \vdots \\ 0 \end{bmatrix}$$

For all other time steps no non-physical terms are created. Therefore we employ

$$\begin{aligned}
i = 0 \qquad & \left(\frac{m}{\delta t^2} + \frac{3\rho c^2 a}{2\delta x} + k\right) u_0^{n+1} - \left(\frac{2\rho c^2 a}{\delta x}\right) u_1^{n+1} + \left(\frac{\rho c^2 a}{2\delta x}\right) u_2^{n+1} = \frac{2m}{\delta t^2} u_0^n - \frac{m}{\delta t^2} u_0^{n-1} + F(t) \\
i = 1 \qquad & (1+2r)u_1^{n+1} - r(u_2^{n+1} + u_0^{n+1}) = 2u_1^n - u_1^{n-1} \\
i = 2 \qquad & (1+2r)u_2^{n+1} - r(u_3^{n+1} + u_1^{n+1}) = 2u_2^n - u_2^{n-1} \\
i = 3 \qquad & (1+2r)u_3^{n+1} - r(u_4^{n+1} + u_2^{n+1}) = 2u_3^n - u_2^{n-1} \\
.... & \\
i = m-2 \qquad & (1+2r)u_{m-2}^{n+1} - r(u_{m-1}^{n+1} + u_{m-3}^{n+1}) = 2u_{m-2} - u_{m-2}^{n-1} \\
i = m-1 \qquad & (1+2r)u_{m-1}^{n+1} - r(u_m^{n+1} + u_{m-2}^{n+1}) = 2u_{m-1}^n - u_{m-1}^{n-1} \\
i = m \qquad & \left(\frac{1}{2\delta t} + \frac{3c}{2\delta x}\right) u_m^{n+1} - \frac{2c}{\delta x} u_{m-1}^{n+1} + \frac{c}{2\delta x} u_{m-2}^{n+1} = \frac{1}{2\delta t} u_m^{n-1}
\end{aligned}$$

Which in turn is transformed to the corresponding sparse matrix.

$$\begin{bmatrix} A & B & C & & \\ 1+2r & -r & & & \\ -r & 1+2r & -r & & \\ & \ddots & \ddots & \ddots & \\ & & -r & 1+2r & -r \\ & & D & E & F \end{bmatrix} \vec{u_i^{n+1}} = \begin{bmatrix} \frac{2}{\delta t^2} \\ 2 \\ \vdots \\ 2 \\ 0 \end{bmatrix} \vec{u_i^n} + \begin{bmatrix} \frac{1}{\delta t^2} \\ -1 \\ \vdots \\ -1 \\ 0 \end{bmatrix} \vec{u_i^{n-1}} + \begin{bmatrix} F(t) \\ 0 \\ \vdots \\ 0 \\ 0 \end{bmatrix}$$

Where

$$\begin{aligned} A_0 &= \frac{2m}{\delta t^2} + \frac{3\rho c^2 a}{\delta x} + k \\ A &= \frac{m}{\delta t^2} + \frac{3\rho c^2 a}{\delta x} + k \\ B &= \frac{-2\rho c^2 a}{\delta x} \\ C &= \frac{\rho c^2 a}{2\delta x} \\ D &= \frac{c}{2\delta x} \\ E &= \frac{-2c}{\delta x} \\ F_0 &= \frac{3c}{2\delta x} \\ F &= \frac{1}{2\delta t} + \frac{3c}{2\delta x} \end{aligned}$$

When this method is implemented in Matlab, we can produce a numerical solution to the PDE. To test the accuracy of this solution, we compared it to an exact solution derived using Laplace transforms. [7]

$$u(0,t) = G + He^{r_1 t} + Ie^{r_2 t} + \sum_{n=1}^{N} \left( J_n \cos(n\omega t) + \frac{K_n}{n\omega} \sin(n\omega t) + L_n e^{r_1 t} + M_n e^{r_2 t} \right) \quad (17)$$

Where

$$
\begin{aligned}
r_{1,2} &= -\frac{\rho ca \pm \sqrt{(\rho ca)^2 - 4mk}}{2m} \\
G &= \frac{aP_m}{mr_1r_2} \\
H &= -\frac{aP_m}{r_1(r_2 - r_1)m} \\
H &= \frac{aP_m}{r_2(r_2 - r_1)m} \\
J_n &= -F_n - G_n \\
K_n &= -r_1F_n - r_2G_n \\
L_n &= \frac{aA_n - mG_n(r_2^2 + n^2\omega^2)}{m(r_1^2 + n^2\omega^2)} \\
M_n &= \frac{a(r_2A_n + n\omega B_n}{m(r_2 - r_1)(r_2^2 + n^2\omega^2)}
\end{aligned}
$$

# 3 Results and Discussion

In this section we will analyze the accuracy of the numerical solution to its analytical counterpart. By plotting the two against one another in Figure 2, we see that the numerical solution follows the curve of the exact solution with little to no visible error. We then perform computational studies, observing the influence of individual parameters on the overall behavior of the system.

## 3.1 Comparison of Numerical and Exact Solution

Here we have chosen the following realistic values to initialize our study: for the CSF, the density has been set to $\rho = 1000$ kg/m$^3$ and $c = 1500$ m/s. For the artery wall, we have chosen mass $m = 0.001$ kg, area $a = 0.01$ m$^2$ and spring constant $k = 8000$ N/m. For the blood pressure, we used P$_m$ =65.7 mmHg, frequency $\omega = 1$ rad/s and harmonics $A_1 = -7.13$, $B_1 = 4.64$, $A_2 = -3.08$, $B_2 = -1.18$, $A_3 = -0.130$, $B_3 = -0.564$, $A_4 = -0.205$, $B_4 = -0.346$, $A_5 = 0.0662$, $B_5 = -0.120$, all in mmHg.

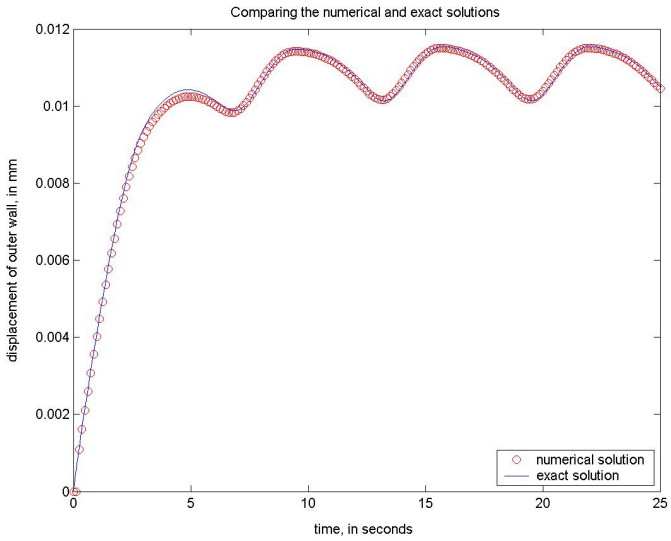


Figure 2: Comparing the Analytical and Numerical Solutions

The data points generated by the numerical solution lie on top of the analytical curve. This suggests that the implicit finite difference methodology was successfully implemented to the orriginal PDE (9-12).

## 3.2 Influence of arterial wall stiffness

The spring constant k models the relative stiffness of the arterial wall and is initially set to 8000 N/m. As this value is decreased, the wall becomes more flexible and will yield more to the force exerted by the blood pressure, moving further into the CSF. Seen in Figure 3, as k is taken from 7000 N/m to 1000 N/m, the outer wall still displays oscillatory behavior, but with greater displacement. The system is also slower to stabilize.

## 3.3 Influence of CSF density

The density of the CSF, $\rho$, has also been taken into account. As the fluid becomes more dense, it will resist the motion of the wall, which should be mathematically observed in a

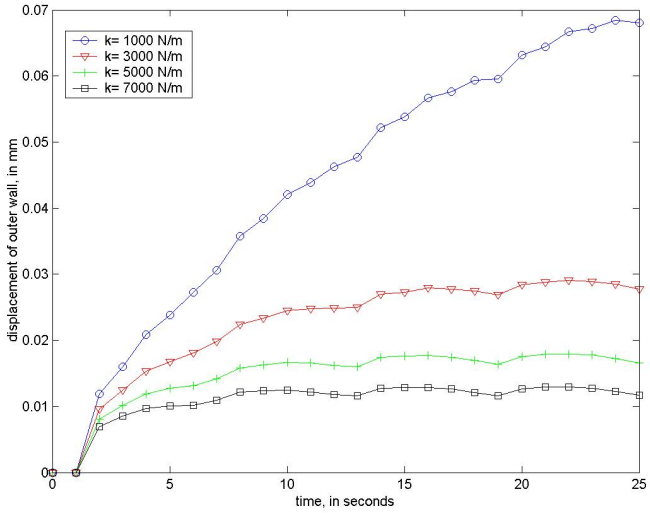


Figure 3: Influence of Wall Stiffness

decreased amplitude in the displacement curve. Initially, we have set the density to 1000 kg/m$^3$. In our computational study, we take the value of $\rho$ from 0 kg/m$^3$ to 2000 kg/m$^3$ and, as expected, see a decreased amplitude. The behavior at $\rho = 0$, is noteworthy in that the smoothness of the curve changes, producing a visible bend. With the numerical

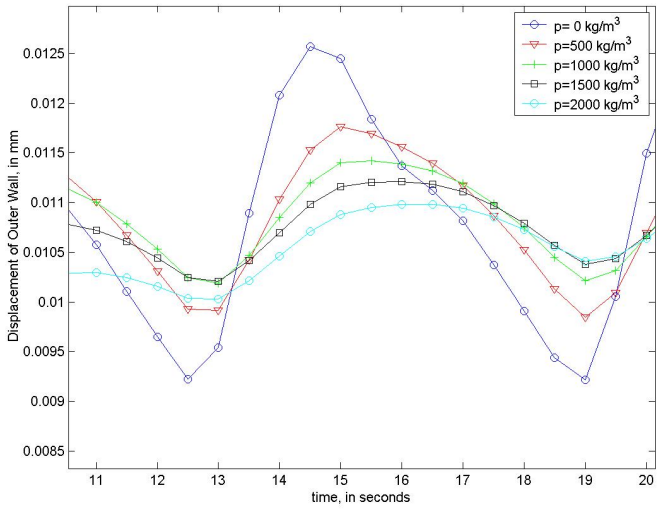


Figure 4: Influence of CSF density

scheme validated, we next attempted to modify the assumptions made in constructing the PDE, specifically the simplification of the Navier-Stokes equation. By making the

model more complex we bring it closer to physical reality. The cerebral spinal fliud was originally assumed to be invicid ($\mu = 0$), giving no resistance to the motion of the outer arterial wall. Allowing $\mu$ to be a constant, we alter (8), giving

$$\rho u_{tt} = \rho c^2 u_{xx} + \mu v_{xx} \tag{18}$$

Using the implicit finite difference method implemented previously, we discritize and move all n+1 terms to the right hand side as follows.

$$\rho\left(\frac{u_i^{n+1} - 2u_i^n + u_i^{n-1}}{\delta t}\right) = \rho c^2\left(\frac{u_{i+1}^{n+1} - 2u_i^{n+1} + u_{i-1}^{n+1}}{\delta x}\right) - \mu\left(\frac{v_{i+1}^{n+1} - 2v_i^{n+1} + v_{i-1}^{n+1}}{\delta x}\right) \tag{19}$$

$$(1+2r)u_i^{n+1} - r(u_{i+1}^{n+1} + u_{i-1}^{n+1}) + \frac{\mu r}{\rho c^2}(v_{i+1}^{n+1} - 2v_i^{n+1} + v_{i-1}^{n+1}) = 2u_i^n - u_i^{n-1} \tag{20}$$

Similar to the previous numerical computation, we applied the boundary and initial conditions to achieve a new system of linear equations and matrices for the first time step and all subsequent time steps. Solving in Matlab with $\mu = 0$ produced the same graph depicted in Figure 2. We would expect that an increase in viscosity would cause the amplitude of the periodic displacement of the wall to decrease. However, as $\mu$ was increased to values up to 10,000 cP, roughly the consistancy of honey, little change was seen in the displacement of the outer arterial wall. This suggests that there is some error in the methodology used. One plausible explaination as to why this scheme fails is that $\mu$ is not constant, changing how we must distritize (15). It is also possible that the discritization of v uses such small steps in space that $v_{i+1}^{n+1} - 2v_i^{n+1} + v_{i-1}^{n+1} = 0$, causing the $\mu v_{xx}$ term to drop from the equation.

# 4 Conclusion and Future Work

This research has constructed a fluid structure interaction model tailored to explore intracranial aneurysms by incorporating its most basic elements— the blood pressure, arte-

rial wall, and CSF — and obtain a numerical solution to the resulting partial differential equation. By using implicit finite differences, we were able to match the numerical and exact solutions, thereby validating the numerical scheme. Future goals will be to modify the assumptions made in the construction of the wave equation and the spring mass system, making the model more complex and physically realistic. Putting aside attempts to include viscosity, the nonlinear terms will be added back into the reduced Navier-Stokes equation. For the spring mass system, a number of alternative models have been suggested, all giving more complex structure and motion to the arterial walls.

# References

[1 P.B. Crompton. Mechanism of growth and rupture in cerebral berry aneurysms.Br. Med J. 1 1138-1142, 1966.]

[2 G.G. Ferguson. Direct Measurement of mean and pulsatile blood pressure at operation in human intracranial saccular aneurysms. Journal of Neurosurgery 36, 560-563, 1972.]

[3 W.R. Milnor. hemodynamics. Williams & Wilkens, Baltimore, 1982.]

[4 T. Sauer. Numerical Analysis. Addison-Wesley, 2005.]

[5 L.N. Sekhar and R.C. Heros. Origin, growth and rupture of saccular aneurysms; a review.Neurosurgery 8, 248-260, 1981.]

[6 A.D. Shah and J.D. Humphrey. Finite strain elastodynamics of intracranial saccular aneurysms. Journal of Biomechanics 32, 593-599, 1999.]

[7 M. Venuti and K. Kelbaugh. Modeling, analysis and computation of fluid structure interaction models for biological systems. 2009.]